PHYSICAL REVIEW D **83,** 094022 (2011)

Discriminating different Z''s via asymmetries at the LHC

Zhong-qiu Zhou,[1,*] Bo Xiao,[1,†] You-kai Wang,[1,‡] and Shou-hua Zhu[1,2,§]

[1]*Institute of Theoretical Physics State Key Laboratory of Nuclear Physics and Technology, Peking University, Beijing 100871, China*
[2]*Center for High Energy Physics, Peking University, Beijing 100871, China*

(Received 14 February 2011; published 19 May 2011)

In practice the asymmetry, which is defined based on the angular distribution of the final states in scattering or decay processes, can be utilized to scrutinize underlying dynamics in and/or beyond the standard model (BSM). As one of the possible BSM physics which might be discovered early at the LHC, extra neutral gauge bosons Z''s are theoretically well motivated. Once Z''s are discovered at the LHC, it is crucial to discriminate different Z''s in various BSM. In principle such a task can be accomplished by measuring the angular distribution of the final states which are produced via Z'-mediated processes. In the real data analysis, asymmetry is always adopted. In the literature several asymmetries have been proposed at the LHC. Based on these works, we stepped further on to study how to optimize the asymmetries in the left-right model and the sequential standard model, as the examples of BSM. In this paper, we examined four kinds of asymmetries, namely, rapidity-dependent forward-backward asymmetry, oneside forward-backward asymmetry, central charge asymmetry, and edge charge asymmetry (see text for details), with $\ell^+\ell^-$ ($\ell = e$, μ), $b\bar{b}$, and $t\bar{t}$ as the final states. In the calculations with $b\bar{b}$ and $t\bar{t}$ final states, the QCD-induced higher-order contributions to the asymmetric cross section were also included. For each kind of final state, we estimated the four kinds of asymmetries and especially the optimal cut usually associated with the definition of the asymmetry. Our numerical results indicated that the capacity to discriminate Z' models can be improved by imposing the optimal cuts.

DOI: 10.1103/PhysRevD.83.094022 PACS numbers: 14.65.Ha, 12.38.Bx

I. INTRODUCTION

The LHC is a powerful machine for discovering a new particle and examining its couplings if the new particle is at $\mathcal{O}$(TeV) or below. In the physics beyond the standard model (BSM), there are usually new particles. For example, in the simplest case, besides the standard model (SM) gauge group $SU(3)_C \otimes SU(2)_L \otimes U(1)_Y$, there can be an extra Abelian gauge group $U(1)$ which implies the existence of the extra gauge boson dubbed as Z'. If the mass of Z' is not so heavy, it can be discovered early at the LHC. Similar to the case of J/ψ discovery, Z' might show up as the di-muon resonance. In fact numerous phenomenological studies on Z' at the LHC have been carried out. After the discovery it is very important to study its spin, couplings, etc. in order to fix the nature of the physics behind the new particle. In principle such detailed information can be obtained via the precise measurement for the angular distributions of the final states into which Z''s decay. However, in practice the asymmetry is usually utilized to investigate the detail properties of the new particle if the data is not abundant. The measurement of the asymmetry at the LEP (Tevatron), as the charge asymmetric electron-positron (proton-antiproton) collider, has shed light on the knowledge of the SM and constrained the BSM severely. The LHC, as the charge symmetric proton-proton collider, needs some special ideas to define and measure the asymmetry.

In the literature, several asymmetry definitions have already been proposed to study the underlying dynamics of the BSM. Note that asymmetry is applicable to all kinds of new physics, not limited to Z'. In this paper Z' is only taken as an example. In order to distinguish different Z' models, forward-backward (FB) asymmetry at the hadron collider is one of the most important tools which was suggested in 1984 in the study of Z' physics [1]. Afterwards, it was widely used in the Z' study [2–28] and has been developed into more convenient forms. In fact, at the LHC there are several other types of asymmetry definitions [29–35]. It is crucial to compare them and find out the most suitable one for the specific purpose, e.g., to study the specific couplings between Z' and the SM fermions. Furthermore, each type of asymmetry definition contains characteristic cuts which should be chosen properly to make the asymmetry most significant. The most suitable type of asymmetry and the most proper cuts associated with asymmetry are different for different physics. In this paper, we are going to investigate the optimal cuts for identifying the Z' in different models at the LHC. In this paper two kinds of Z' test models, namely, the left-right (LR) and sequential standard model (SSM) are adopted.

In the previous study [8], the authors utilized the forward-backward asymmetry defined by themselves in order to identify the different Z''s, which can decay into $\mu^+\mu^-(e^+e^-)$, $b\bar{b}$ as well as $t\bar{t}$. For the final states of $\mu^+\mu^-(e^+e^-)$, asymmetry is calculated for the on-peak

*zhongqiu_zhou@pku.edu.cn
†homenature@pku.edu.cn
‡wangyk@pku.edu.cn
§shzhu@pku.edu.cn

data sample, namely, the invariant mass of the charged lepton pair lying within $M_{Z'} - 3\Gamma$ and $M_{Z'} + 3\Gamma$, as well as the off-peak data sample with invariant mass lying within $2/3M_{Z'}$ and $M_{Z'} - 3\Gamma$. Here Γ is the total width of Z'. For the $b\bar{b}$ and $t\bar{t}$ final states, only asymmetry of the on-peak data sample with quark pair invariant mass within $M_{Z'} - 2.5\Gamma$ and $M_{Z'} + 2.5\Gamma$ was calculated. In this paper we extended the above analysis to more asymmetries defined recently, namely, oneside forward-backward asymmetry, central charge asymmetry, and edge charge asymmetry. In our calculation for the quarks as the final states, we included also the contributions from the higher-order QCD-induced effects. Moreover we investigated the optimal conditions which make the asymmetry more significant. Explicitly, in our paper we are going to scrutinize which type of asymmetry and the corresponding cuts are the most suitable ones for the $\mu^+\mu^-(e^+e^-)$ on/off-peak events and the $b\bar{b}$ and $t\bar{t}$ events, respectively.

In Sec. II, different asymmetries at the LHC are briefly described. In Sec. III, we first calculated four types of asymmetries at the LHC with their characteristic cuts for the $\mu^+\mu^-(e^+e^-)$ on/off-peak events, $b\bar{b}$, $t\bar{t}$ on-peak events, respectively. Second, based on the calculations we optimize the asymmetry for each case by choosing different cuts. Third, we showed how to discriminate different Z''s in LR and SSM models utilizing the optimized asymmetry. In Sec. IV, we gave our discussions and conclusions.

II. ASYMMETRY AT THE LHC

The LHC is the symmetric proton-proton collider, thus the usual defined asymmetry is absolute zero after integrating all kinematical regions. However, if one selects events in a certain kinematical region, the asymmetry arising at the partonic level will be kept.

A. Forward-backward asymmetry for the partonic level process $q\bar{q} \to f\bar{f}$

In order to illustrate the Z' contribution to asymmetry, we describe firstly the forward-backward asymmetry in the SM. At the tree level in the SM, the FB asymmetry of $q\bar{q} \to Z/\gamma^* \to l\bar{l}$ gets contributions from the self-conjugation of the Z-induced s-channel feynman diagram

$$\frac{d\sigma}{d\cos\theta} \propto \frac{g^4 s^2}{c_W^4[(s - M_Z^2)^2 + \Gamma_Z^2 M_Z^2]}[((g_L^l)^2 + (g_R^l)^2)((g_L^q)^2 + (g_R^q)^2)(1 + \cos^2\theta) + 2((g_L^l)^2 - (g_R^l)^2)((g_L^q)^2 - (g_R^q)^2)\cos\theta], \quad (1)$$

and the interference between this diagram and the γ-induced s-channel feynman diagram

$$\frac{d\sigma}{d\cos\theta} \propto \frac{g^2 e e_q (M_Z^2 - s)s}{c_W^2[(s - M_Z^2)^2 + \Gamma_Z^2 M_Z^2]}[2(g_L^l + g_R^l)(g_L^q + g_R^q) \times (1 + \cos^2\theta) + 4(g_L^l - g_R^l)(g_L^q - g_R^q)\cos\theta]. \quad (2)$$

Around the Z pole, the FB asymmetry is almost determined by the first contribution, while off the Z pole, the second contribution plays an important role.

After introducing Z', the situation becomes a little bit complicated. On the Z' pole, if the coupling of the Z' to fermions is not purely vectorlike nor purely axial-vector–like, namely, $|g_L^f| = |g_R^f|$, there will be a nonzero contribution to FB asymmetry from the self-conjugation of the Z' induced s-channel feynman diagram. Otherwise the contribution from the self-conjugation of Z' to FB asymmetry will be zero. However, for the data sample off the Z' pole, FB asymmetry will be nonzero due to the interference of the Z' diagram and the SM Z/γ^* induced s-channel feynman diagrams.

From the above description, we can see clearly that the FB asymmetry relates tightly to the chiral properties of the couplings and how to select data samples. In the BSM which contains the Z', the coupling of Z' and SM fermions is usually different. How to extract the corresponding couplings via an asymmetry measurement and subsequently discriminate different BSM is the key motivation for both the theoretical and experimental studies.

The above formulas are applicable also to $q\bar{q} \to b\bar{b}(t\bar{t})$, however there are additional important contributions to the FB asymmetry from the QCD high-order processes [29,30]. If one selects the events around the Z' pole, the QCD high-order contributions are suppressed. However, such an effect will be important for the asymmetry of off-pole events. In this paper, such QCD-induced contributions will be included in the analysis.

B. Four asymmetries defined at the LHC

The proton-proton collider LHC is forward-backward charge symmetric, so the asymmetry of the fermion pairs produced at the LHC is null if integrating over the full phase space. However, by imposing some kinematical cuts, the asymmetry generated at the partonic level $q\bar{q} \to f\bar{f}$ can be kept. Different types of asymmetries have been defined. The above-mentioned FB asymmetry [1–10], which has been frequently used in Z' studies, contains a characteristic fermion pair rapidity $Y_{f\bar{f}}$ cut. We refer it as rapidity-dependent forward-backward asymmetry (A_{RFB}) throughout this paper. The other three asymmetries which will be investigated in this paper are oneside forward-backward asymmetry (A_{OFB}) [33,34], central charge asymmetry (A_C) [29–32], and edge charge asymmetry (A_E) [35]. We collect their definitions as below

$$A_{RFB}(Y_{f\bar{f}}^{cut}) = \frac{\sigma(|Y_f| > |Y_{\bar{f}}|) - \sigma(|Y_f| < |Y_{\bar{f}}|)}{\sigma(|Y_f| > |Y_{\bar{f}}|) + \sigma(|Y_f| < |Y_{\bar{f}}|)}\Big|_{|Y_{f\bar{f}}| > Y_{f\bar{f}}^{cut}}, \quad (3)$$

$$A_{OFB}(p_{Z,f\bar{f}}^{cut}) = \frac{\sigma(|Y_f| > |Y_{\bar{f}}|) - \sigma(|Y_f| < |Y_{\bar{f}}|)}{\sigma(|Y_f| > |Y_{\bar{f}}|) + \sigma(|Y_f| < |Y_{\bar{f}}|)}\Big|_{|p_{z,f\bar{f}}| > p_{Z,f\bar{f}}^{cut}}, \quad (4)$$

$$A_C(Y_C) = \frac{\sigma_f(|Y_f| < Y_C) - \sigma_{\bar{f}}(|Y_{\bar{f}}| < Y_C)}{\sigma_f(|Y_f| < Y_C) + \sigma_{\bar{f}}(|Y_{\bar{f}}| < Y_C)}, \quad (5)$$

$$A_E(Y_C) = \frac{\sigma_f(Y_C < |Y_f|) - \sigma_{\bar{f}}(Y_C < |Y_{\bar{f}}|)}{\sigma_f(Y_C < |Y_f|) + \sigma_{\bar{f}}(Y_C < |Y_{\bar{f}}|)}, \quad (6)$$

in which Y is the rapidity of the $f/\bar{f}$ or fermion pair, accordingly. The $p_{z,f\bar{f}}$ is the z-direction momentum of the fermion pair.

In order to keep the partonic asymmetry even at the hadronic level, no matter how different these asymmetries look, each of them has used the fact that the energy fraction of the valence quark is usually larger than that of the sea quark in the proton. These asymmetries can be classified into two categories according to their similarities. A_C and A_E belong to one category and the remaining two belong to the other. For A_C and A_E, they account two complementary kinematical regions, namely, the central region $|Y_{f,\bar{f}}| < Y_C$ and the edge region $|Y_{f,\bar{f}}| > Y_C$ in the laboratory frame, respectively. A_E can usually suppress more efficiently the symmetric $gg \to q\bar{q}$ background events which mostly distribute in the central region [35]. Therefore, the A_E is usually more significant than the A_C. The difference between A_{RFB} and A_{OFB} is the cuts in order to keep the partonic asymmetry. $Y_{f\bar{f}}$ and $P^z_{f\bar{f}}$ are proportional to $(x_1 - x_2)/(x_1 + x_2)$ and $(x_1 - x_2)$, respectively, where x_1 and x_2 are the momentum fraction of the two colliding partons. The most important difference between the two categories is that the asymmetry utilizes the different kinematical information. The asymmetries in the first category utilize either f or $\bar{f}$ momentum information. While the asymmetries of the second category require us to measure the kinematical information of f and $\bar{f}$ simultaneously.

Because of their different characteristics, the four types of asymmetries will be used in different cases. Each of them have their most suitable places. In the followings, we will investigate how to use four asymmetries to discriminate different Z' models, namely, which one is the most suitable type of asymmetry and the corresponding optimal cuts.

III. DISCRIMINATING DIFFERENT Z'S VIA ASYMMETRIES

A. Z' in the left-right model and sequential standard model

In this paper, in order to illustrate how to utilize asymmetries to discriminate different Z''s, we choose two test models as the examples: the left-right model and sequential standard model.

The left-right model is based on the symmetry group $SU(2)_R \times SU(2)_L \times U(1)_{B-L}$, where $B - L$ is the difference between baryon and lepton numbers. The couplings between the Z' and fermions are [4,6]

TABLE I. Couplings of the Z' boson to the SM fermions in the left-right model and the sequential SM. $\alpha_{LR} = \sqrt{(c_W^2 g_R^2 / s_W^2 g_L^2) - 1}$, where $g_L = e/s_W$ and g_R are the $SU(2)_L$ and $SU(2)_R$ coupling constants with $s_W^2 = 1 - c_W^2 \equiv \sin^2\theta_W$ [4].

f	$g_L^{fZ'}$	$g_R^{fZ'}$	g_V^f	g_A^f
e	$\frac{1}{2\alpha_{LR}}$	$\frac{1}{2\alpha_{LR}} - \frac{\alpha_{LR}}{2}$	$-\frac{1}{2} + 2\sin^2\theta_W$	$-\frac{1}{2}$
u	$-\frac{1}{6\alpha_{LR}}$	$-\frac{1}{6\alpha_{LR}} + \frac{\alpha_{LR}}{2}$	$\frac{1}{2} - \frac{4}{3}\sin^2\theta_W$	$\frac{1}{2}$
d	$-\frac{1}{6\alpha_{LR}}$	$-\frac{1}{6\alpha_{LR}} - \frac{\alpha_{LR}}{2}$	$-\frac{1}{2} + \frac{2}{3}\sin^2\theta_W$	$-\frac{1}{2}$

$$g_{Z'} J^\mu_{Z'} Z'_\mu = \frac{e}{c_W} \sum_f \bar{\psi}_f \gamma^\mu \left[\frac{1 - \gamma^5}{2} g_L^{fZ'} + \frac{1 + \gamma^5}{2} g_R^{fZ'} \right] \psi_f Z'_\mu. \quad (7)$$

As the test model, the sequential standard model Z' has the same fermion couplings as the SM Z boson and which can be written as

$$g_{Z'} J^\mu_{Z'} Z'_\mu = -\frac{g}{2c_W} \sum_f \bar{\psi}_f \gamma_\mu (g_V^f - g_A^f \gamma_5) \psi_f Z'_\mu. \quad (8)$$

The parameters in these two models can be summarized in Table I. Throughout the paper the mass of Z' is set to be 1.5 TeV for both models. The α_{LR} in the LR model is set to be 1.88 as the benchmark point, in order to make the width of Z' in the LR model the same as that in the SSM. SM parameters are chosen as $\alpha = 1/127.9$, $\sin^2\theta_W = 0.231$, $M_Z = 91.133$ GeV, $\Gamma_Z = 2.495$ GeV, and $m_t = 171.2$ GeV. In calculating the width of the Z', only its decays to the SM fermions are included.

B. Optimizing asymmetry

In our analysis, the basic kinematical cuts are taken as $p_T > 20$ GeV and $Y < 2.5$ for the leptons, $p_T > 0.3 M_{Z'}$ and $Y < 2.5$ for the bottom and top quarks. Here the p_T cut for quarks can suppress the QCD backgrounds. The LHC energy $\sqrt{s}$ is set to be 14 TeV.

Figure 1 shows A_{RFB} for the process $pp \to e^+e^-X$ as a function of $M_{e^+e^-}$. From the figure it is clear that the asymmetry depends on $M_{e^+e^-}$. As depicted above, the asymmetry depends on the chiral properties of Z' and SM fermions, as well as the selected data sample. In order to keep as much asymmetry information as possible, in our analysis the four data samples are chosen, just as with those in Ref. [8]. They are the on-peak events with $M_{Z'} - 3\Gamma < M_{\mu^+\mu^-(e^+e^-)} < M_{Z'} + 3\Gamma$, off-peak events with $2/3 M_{Z'} < M_{\mu^+\mu^-(e^+e^-)} < M_{Z'} - 3\Gamma$, on-peak events with $M_{Z'} - 2.5\Gamma < M_{b\bar{b}} < M_{Z'} + 2.5\Gamma$, and on-peak events with $M_{Z'} - 2.5\Gamma < M_{t\bar{t}} < M_{Z'} + 2.5\Gamma$.

From Fig. 1 A_{RFB} with $Y^{cut}_{f\bar{f}} = 0.35$ is larger than that with $Y^{cut}_{f\bar{f}} = 0$. However, the magnitude of A_{RFB} is not a good measure to optimize the observable. As usual we

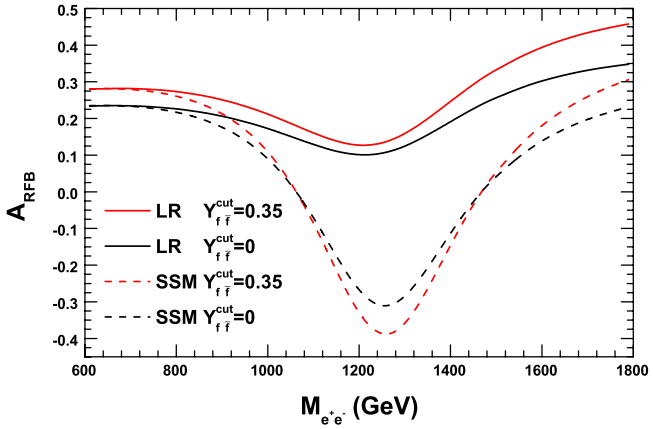

FIG. 1 (color online). A_{RFB} for the process $pp \to e^+e^-X$ as a function of $M_{e^+e^-}$ in the LR mode and SSM with cuts $Y^{cut}_{f\bar{f}} = 0$ and $Y^{cut}_{f\bar{f}} = 0.35$, respectively.

utilize the significance of the asymmetry as a measure to select optimal cuts. The significance is defined as

$$S_A \equiv \frac{\sigma^A \mathcal{L}}{\sqrt{\sigma \mathcal{L}}} = A_{FB}\sqrt{\mathcal{L}\sigma}, \tag{9}$$

where A_{FB} can be A_{RFB}, A_{OFB}, A_C, or A_E; $\mathcal{L}$ is the LHC integrated luminosity which is taken as 100 fb^{-1} throughout our analysis; and σ is the cross section. Note that the detection efficiency is not included in the definition equation (9) because we only utilize this simple variable to optimize asymmetries and the corresponding cuts, and the efficiency choice is irrelevant for this purpose.

Figures 2–5, show the significance as a function of the corresponding cut for four asymmetries and four data samples, respectively. In order to achieve the maximum significance the corresponding best cuts are depicted in Tables II, III, IV, and V, respectively.

Generally speaking, the significance of the LR model is always greater than that of the SSM in the benchmark parameters we choose. S_{RFB} and S_{OFB} are not so sensitive to the cuts as those of S_C and S_E. Their maximum values are almost the same. At the same time the optimized cuts are the same for the two test models although their magnitudes are different. The reason is that the optimal cuts depend mainly on the properties of the parton distribution function and mass of the Z'. Therefore, the optimal cuts are nearly independent of the chiral properties of Z' coupling to fermions. The optimized cuts obtained from one specific Z' model are applicable to any other Z' model with the same Z' mass.

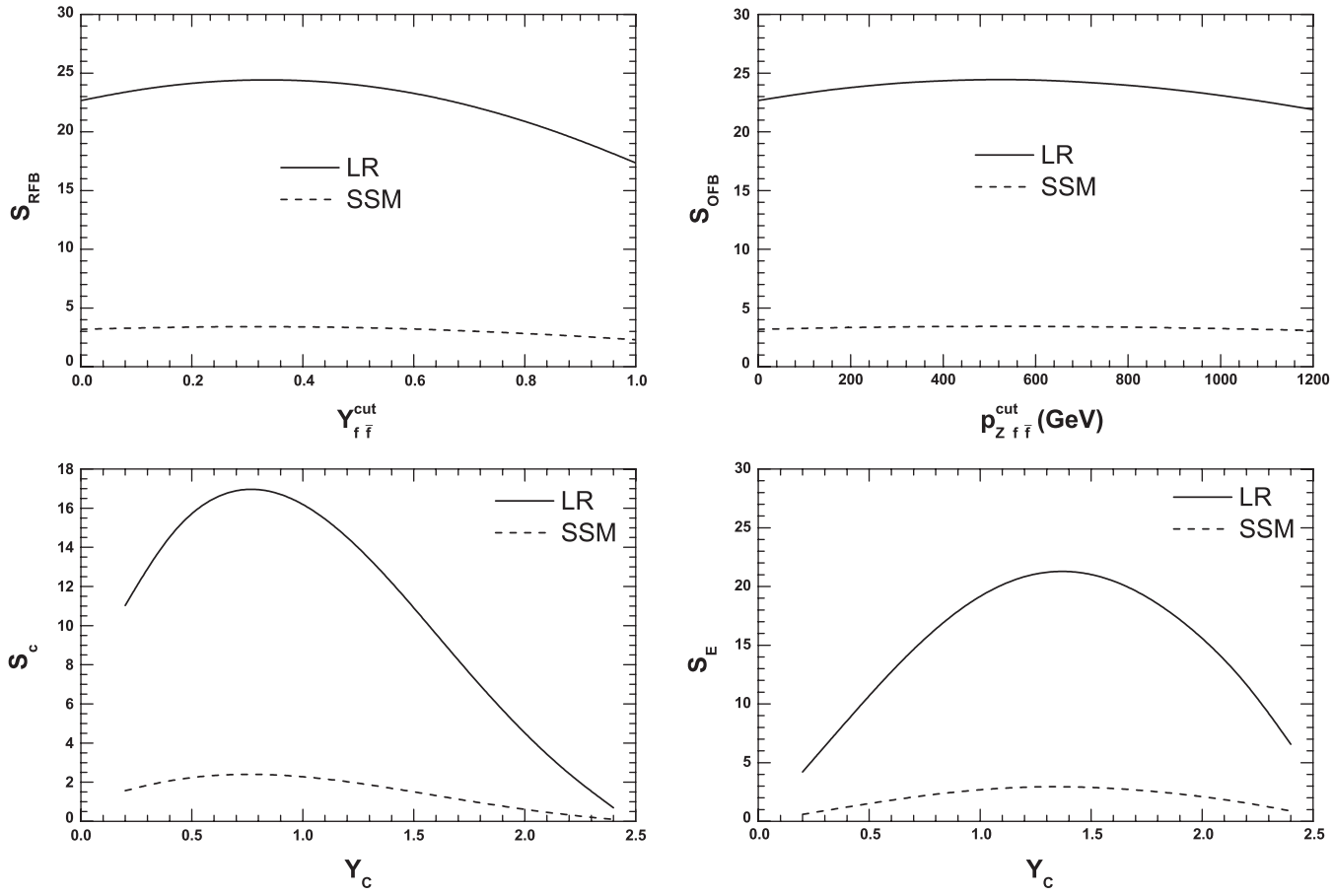

FIG. 2. The significance as a function of the corresponding cut for on-peak e^+e^- events in LR model and SSM is shown.

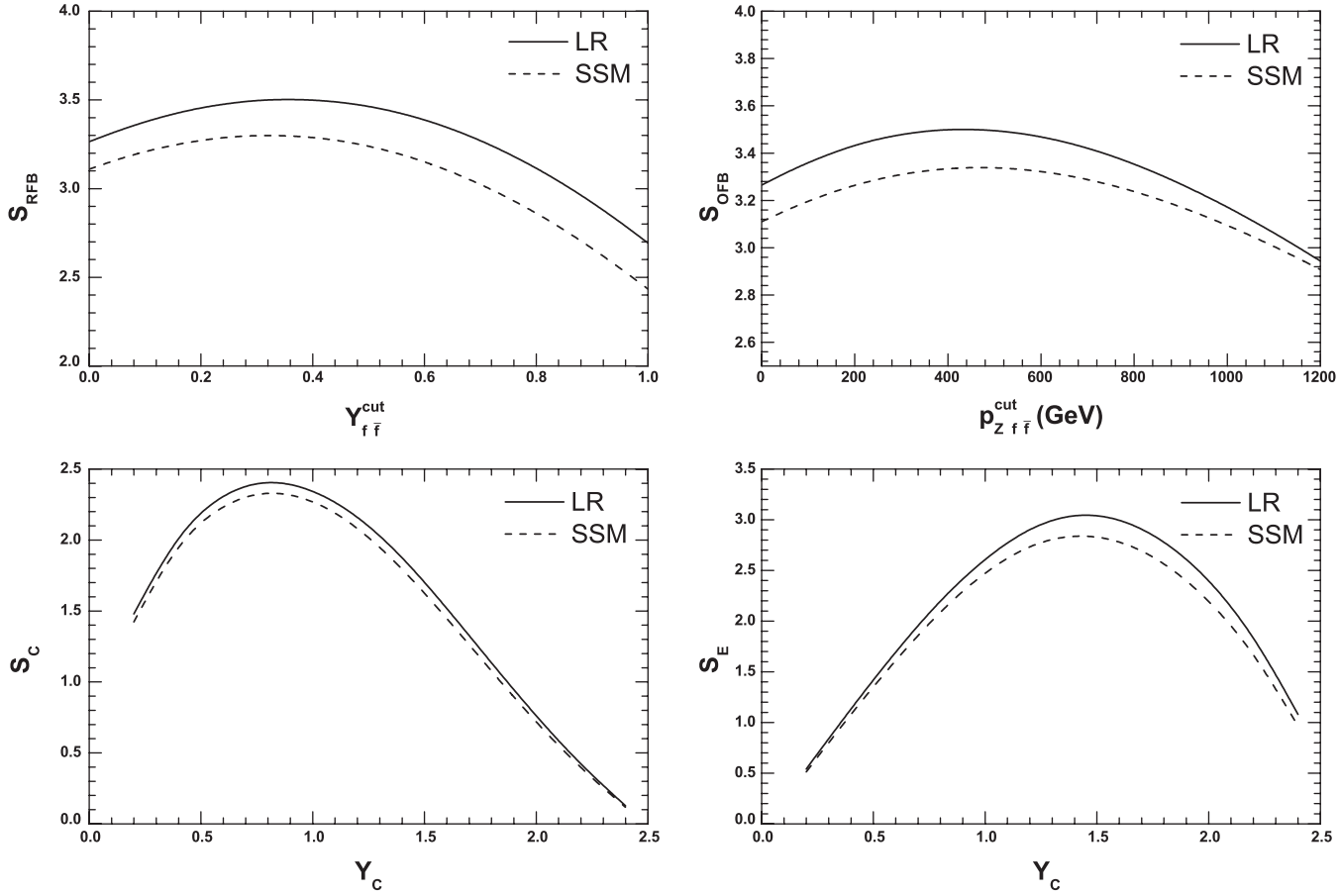

FIG. 3. Same as Fig. 2 except for off-peak e^+e^- events.

In the LR model or SSM, A_{OFB} and A_{RFB} can obtain almost the same highest significance values. The significance of A_E is smaller and the significance of A_C is the smallest. The reason is that A_E and A_C defined in the laboratory frame are diluted by the longitudinal boosts from the partonic level to the hadron level. A_C is even smaller because it includes more symmetric backgrounds than that of A_E. Note that these results are based on the assumption that the final $f\bar{f}$ pair can be completely reconstructed. In the real experiment, taking the top quark pair as the example, the momentum precision of the top pair will be limited by the missing neutrino when using the top semileptonically decaying mode [36]. While A_E and A_C can be free from this problem because they utilize only the top or antitop hadronic decay mode.

C. Discriminating Z' models utilizing the optimized asymmetry

Based on the optimal cuts obtained above, we can discriminate different Z''s via the precise asymmetry measurements at the LHC. In this part we calculated the asymmetries and compare the optimal and unoptimal cases. The results for all asymmetries can be deduced in the same procedure. Note that the optimized cuts are almost the same for different Z' models provided that the Z' mass is the same.

To identify the candidate Z' model, the measured asymmetry should be compared with the theoretical predictions. In our analysis, asymmetries by theoretical predictions with errors are presented as the two-dimensional plot, similar to that in Ref. [8].

In Fig. 6 we show the different asymmetries for both the LR model and the SSM. Central values are calculated in both optimized and unoptimized cases. The statistic error of forward-backward asymmetry A_{FB} is obtained from the statistics study, and the formula is

$$\Delta A_{FB} \equiv \sqrt{\frac{4N^F N^B}{N^3}} = \frac{1}{\sqrt{N}}\sqrt{1-\left(\frac{N^A}{N}\right)^2} \cong \frac{1}{\sqrt{\mathcal{L}\sigma\epsilon_{f\bar{f}}}}. \quad (10)$$

Here N^F/N^B are numbers of forward/backward events, and $N^A = N^F - N^B$ ($N = N^F + N^B$) are the number of asymmetric (total) events. The significance after including reconstruction efficiency is

$$S^{\epsilon}_A \equiv \frac{\sigma^A \mathcal{L}\epsilon_{f\bar{f}}}{\sqrt{\sigma\mathcal{L}\epsilon_{f\bar{f}}}} = A_{FB}\sqrt{\mathcal{L}\sigma\epsilon_{f\bar{f}}}. \quad (11)$$

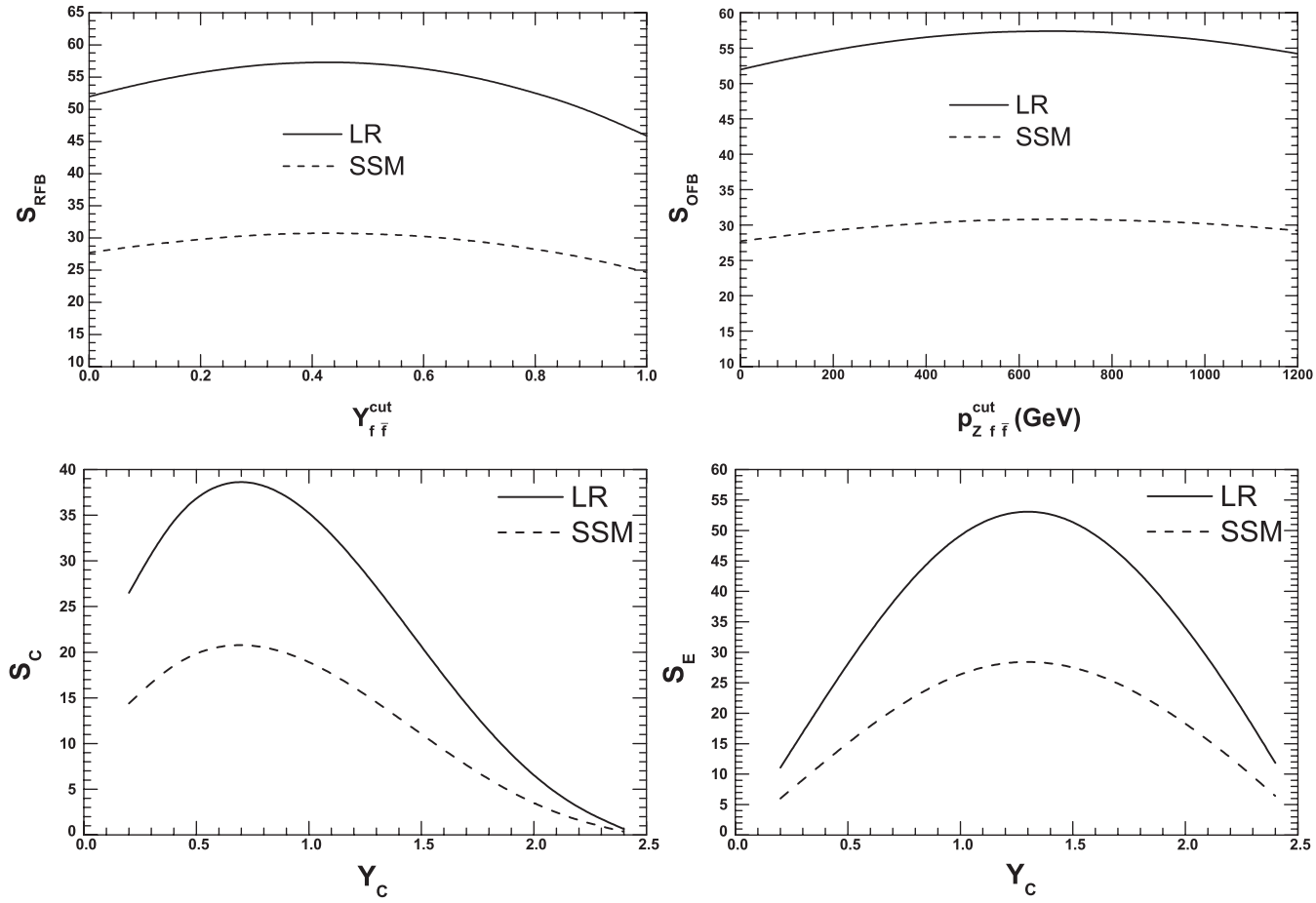

FIG. 4. Same as Fig. 2 except for on-peak $b\bar{b}$ events.

From Eq. (10) and (11) we can see that $S_A^{\epsilon} = \mathrm{A_{FB}}/\Delta\mathrm{A_{FB}}$. In our estimation, the $b\bar{b}$ and $t\bar{t}$ reconstruction efficiencies are taken as $\epsilon_{b\bar{b}} = 0.36$ and $\epsilon_{t\bar{t}} = 0.075$, respectively, [8]. For the $b\bar{b}$ and $t\bar{t}$ final states, the next-to-leading order QCD contribution to the asymmetric cross sections are included. For the $b\bar{b}$ final state, the QCD next-to-leading order contribution to on-peak $\mathrm{A_{RFB}}$ is 1.38% for the optimized case and 0.96% for the unoptimized $Y^{f\bar{f}}_{\mathrm{cut}} = 0$ case. The contribution is a little bit larger than the statistic error (see the left-bottom diagram of Fig. 6), so this effect should be taken into account. For the $t\bar{t}$ final states, the QCD next-to-leading order contribution to on-peak $\mathrm{A_E}$ is 0.53% for the optimized case, which is much less than the statistic error (see the right-bottom diagram of Fig. 6), so this effect can be neglected.

From the Fig. 6, the two models give the apparently different predictions for two asymmetries. Even without optimal cuts, the asymmetries can be utilized to discriminate models in this case. However in the real case, the asymmetry difference for various models might be small. In this case the optimal cuts can help to improve the capacity to discriminate models. From the figure it is obviously that the central values of the asymmetries separate more in both the LR model and the SSM. However, due to the decreasing of the statistics, the error bar becomes a little bit larger for the optimized case.

IV. DISCUSSIONS AND CONCLUSIONS

In this paper we investigated how to utilize the asymmetry measurements at the LHC to discriminate underlying dynamics, by taking Z' model as the example. Unlike LEP and Tevatron, the LHC is a symmetric proton-proton collider, thus the asymmetry at the LHC has the unique feature which should be studied in detail. In the literature several asymmetries have been proposed at the LHC, namely, rapidity-dependent forward-backward asymmetry, oneside forward-backward asymmetry, central charge asymmetry, and edge charge asymmetry, with $\ell^+\ell^-$, $b\bar{b}$, and $t\bar{t}$ as the final states. Based on these works, we stepped further on to analyze how to optimize the asymmetries in the left-right model and the sequential standard model. In the calculations with $b\bar{b}$ and $t\bar{t}$ final states, the QCD-induced higher-order contributions to the asymmetric cross section were also included. For each kind of final state, we estimated the four kinds of asymmetries and especially the optimal cuts usually associated with the definition of the

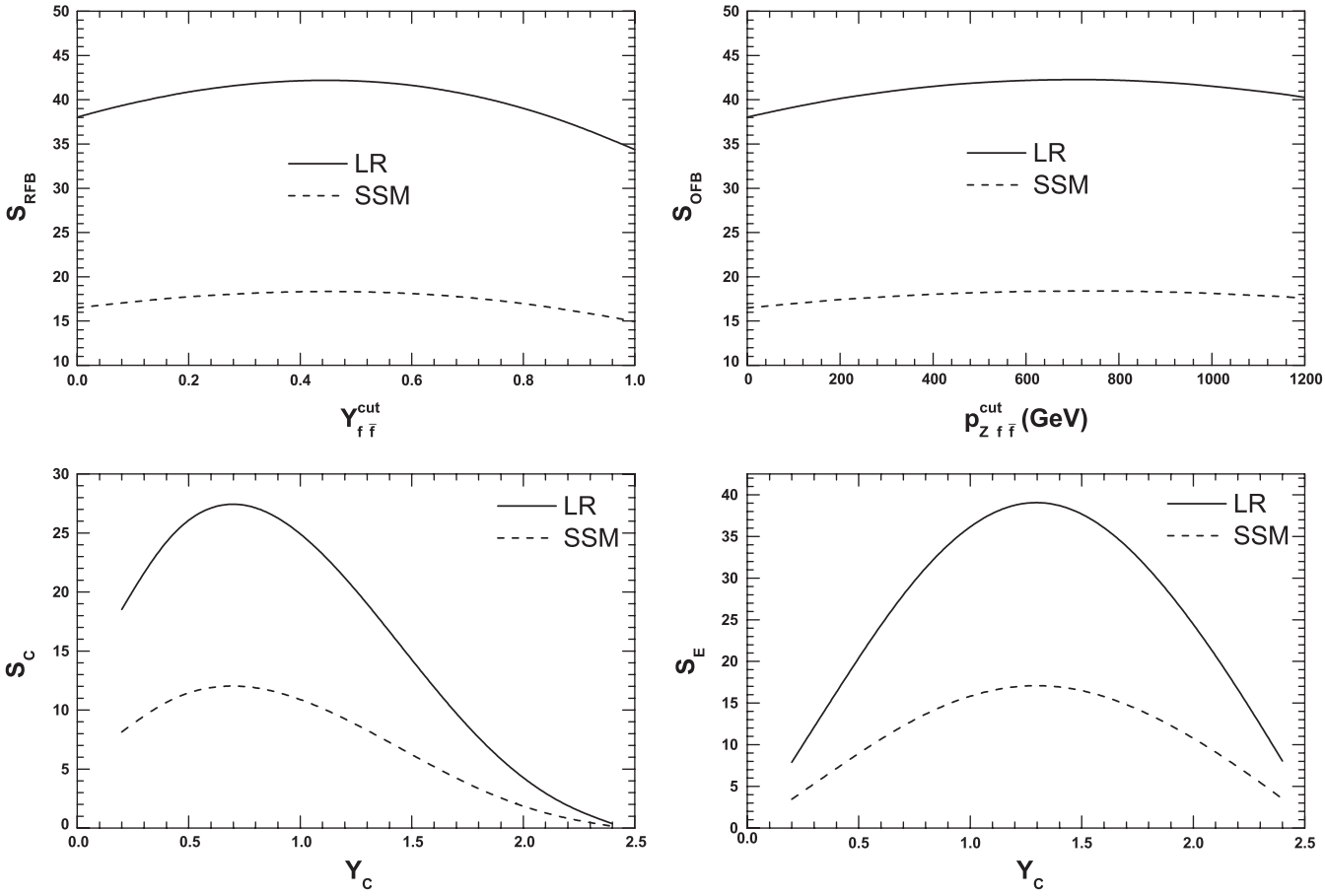

FIG. 5. Same as Fig. 2 except for on-peak $t\bar{t}$ events.

TABLE II. The optimized cut and the corresponding maximum value of significance for on-peak e^+e^- events for the four kinds of asymmetries in both LR model and SSM are shown.

LR	A_{RFB}	A_{OFB}	A_C	A_E
Best cut	$Y^{f\bar{f}}_{cut} = 0.35$	$P^{f\bar{f}}_{z,cut} = 550$ GeV	$Y_C = 0.8$	$Y_C = 1.4$
Significance (with 100 fb^{-1})	24.4	24.4	17.1	21.5
SSM	A_{RFB}	A_{OFB}	A_C	A_E
Best cut	$Y^{f\bar{f}}_{cut} = 0.35$	$P^{f\bar{f}}_{z,cut} = 550$ GeV	$Y_C = 0.8$	$Y_C = 1.4$
Significance (with 100 fb^{-1})	3.40	3.43	2.43	2.97

TABLE III. The same as Table II except for off-peak e^+e^- events.

LR	A_{RFB}	A_{OFB}	A_C	A_E
Best cut	$Y^{f\bar{f}}_{cut} = 0.35$	$P^{f\bar{f}}_{z,cut} = 450$ GeV	$Y_C = 0.8$	$Y_C = 1.4$
Significance (with 100 fb^{-1})	3.51	3.51	2.43	3.07
SSM	A_{RFB}	A_{OFB}	A_C	A_E
Best cut	$Y^{f\bar{f}}_{cut} = 0.35$	$P^{f\bar{f}}_{z,cut} = 450$ GeV	$Y_C = 0.8$	$Y_C = 1.4$
Significance (with 100 fb^{-1})	3.30	3.34	2.36	2.87

TABLE IV. The same as Table II except for on-peak $b\bar{b}$ events.

LR	A_{RFB}	A_{OFB}	A_C	A_E
Best cut	$Y^{f\bar{f}}_{cut} = 0.45$	$P^{f\bar{f}}_{z,cut} = 700$ GeV	$Y_C = 0.6$	$Y_C = 1.2$
Significance (with 100 fb^{-1})	57.2	57.4	38.8	53.1
SSM	A_{RFB}	A_{OFB}	A_C	A_E
Best cut	$Y^{f\bar{f}}_{cut} = 0.45$	$P^{f\bar{f}}_{z,cut} = 700$ GeV	$Y_C = 0.6$	$Y_C = 1.2$
Significance (with 100 fb^{-1})	30.7	30.8	20.9	28.5

TABLE V. The same as Table II except for on-peak $t\bar{t}$ events.

LR	A_{RFB}	A_{OFB}	A_C	A_E
Best cut	$Y^{f\bar{f}}_{cut} = 0.45$	$P^{f\bar{f}}_{z,cut} = 700$ GeV	$Y_C = 0.6$	$Y_C = 1.2$
Significance (with 100 fb^{-1})	42.2	42.3	27.6	39.2
SSM	A_{RFB}	A_{OFB}	A_C	A_E
Best cut	$Y^{f\bar{f}}_{cut} = 0.45$	$P^{f\bar{f}}_{z,cut} = 700$ GeV	$Y_C = 0.6$	$Y_C = 1.2$
Significance (with 100 fb^{-1})	18.3	18.4	12.1	17.1

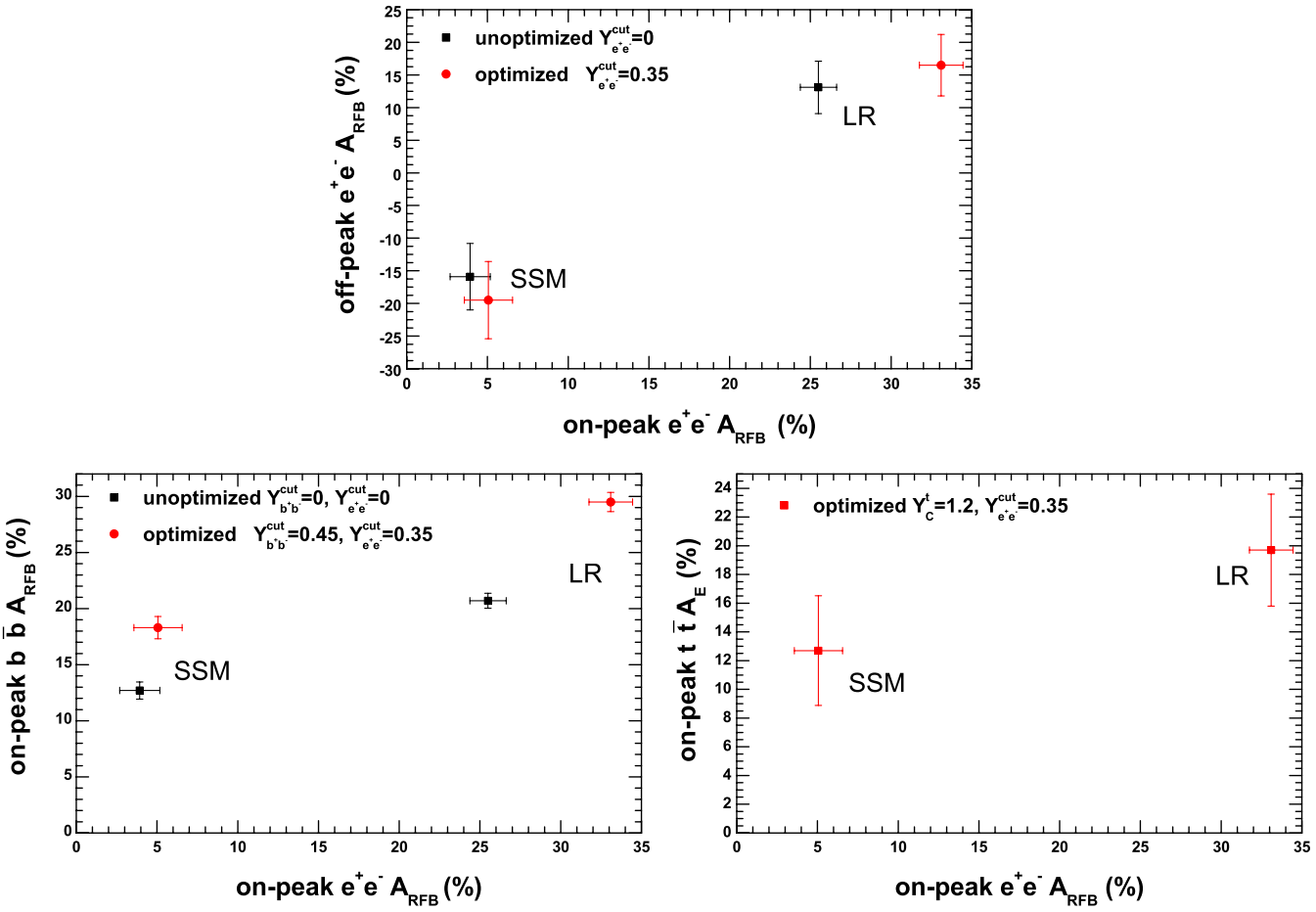

FIG. 6 (color online). Two-dimensional plots of asymmetries A_{RFB}'s for off- and on-peak e^+e^- events, A_{RFB}'s for on-peak $b\bar{b}$ and e^+e^- events, and A_E and A_{RFB} for on-peak $t\bar{t}$ and e^+e^- events, respectively. Both optimized and unoptimized results for A_{RFB} and optimized ones for A_E with error bars in the LR model and SSM are presented.

asymmetry. Our studies showed that the optimal cut is stable for different Z' models provided that the Z' mass is equal. The numerical results indicated that the capacity to discriminate Z' models can be improved by imposing the optimal cuts.

In this paper only Z' models of left-right and the sequential standard model were investigated as the examples. However, the optimization obtained from these two examples is suitable for any kind of Z' models provided that they have the same Z' mass. The Z' mass throughout this paper is assumed to be 1.5 TeV as the benchmark parameter. If the Z' mass is other than 1.5 TeV, the optimal condition should be investigated in the same procedure. Moreover, the precise asymmetry measurement at the LHC can be utilized to scrutinize any new dynamics beyond the standard model, not limited to the Z' case.

ACKNOWLEDGMENTS

This work was supported in part by the Natural Science Foundation of China (Grant No 11075003).

[1] P. Langacker, R. W. Robinett, and J. L. Rosner, Phys. Rev. D **30**, 1470 (1984).
[2] M. Cvetic and S. Godfrey, in *Electroweak Symmetry Breaking and New Physics at the TeV Scale* edited by T. L. Barklow *et al.* (World Scientific, Singapore, 1995) [arXiv:hep-ph/9504216].
[3] M. Dittmar, Phys. Rev. D **55**, 161 (1997).
[4] M. Dittmar, A.-S. Nicollerat, and A. Djouadi, Phys. Lett. B **583**, 111 (2004).
[5] S. Godfrey and T. A. W. Martin, Phys. Rev. Lett. **101**, 151803 (2008).
[6] F. Petriello and S. Quackenbush, Phys. Rev. D **77**, 115004 (2008).
[7] P. Langacker, Rev. Mod. Phys. **81**, 1199 (2009).
[8] R. Diener, S. Godfrey, and T. A. W. Martin, arXiv:0910.1334.
[9] R. Diener, S. Godfrey, and T. A. W. Martin, Phys. Rev. D **80**, 075014 (2009).
[10] R. Diener, S. Godfrey, and T. A. W. Martin, arXiv:1006.2845.
[11] V. Barger and K. Whisnant, Phys. Rev. D **36**, 979 (1987).
[12] F. del Aguila, M. Quiros, and F. Zwirner, Nucl. Phys. **B287**, 419 (1987).
[13] V. Barger, N. G. Deshpande, J. L. Rosner, and K. Whisnant, Phys. Rev. D **35**, 2893 (1987).
[14] U. Baur and K. H. Schwarzer, Phys. Lett. B **180**, 163 (1986).
[15] S. Godfrey, J. L. Hewett, and T. G. Rizzo, Phys. Rev. D **37**, 643 (1988).
[16] J. L. Rosner, Phys. Lett. B **221**, 85 (1989).
[17] F. Boudjema, F. M. Renard, and C. Verzegnassi, Phys. Lett. B **202**, 411 (1988).
[18] J. D. Anderson, M. H. Austern, and R. N. Cahn, Phys. Rev. D **46**, 290 (1992).
[19] M. Cvetic and P. Langacker, Phys. Rev. D **46**, R14 (1992).
[20] P. Langacker and M. Luo, Phys. Rev. D **45**, 278 (1992).
[21] F. Feruglio, 26th Rencontres de Moriond, Les Arcs, France, 1991, http://ccdb4fs.kek.jp/cgi-bin/img/allpdf?199106081.
[22] C. Verzegnassi, Beyond the Standard Model, Int. Europhysics Conf. on High Energy Physics, Uppsala, Sweden, 1987, http://ccdb4fs.kek.jp/cgi-bin/img/allpdf?198801469.
[23] J. L. Rosner, Phys. Rev. D **35**, 2244 (1987).
[24] J. L. Rosner, Phys. Rev. D **54**, 1078 (1996).
[25] F. del Aguila, M. Cvetič, and P. Langacker, Phys. Rev. D **48**, R969 (1993).
[26] J. Abdallah *et al.* (DELPHI Collaboration), Eur. Phys. J. C **45**, 589 (2006).
[27] P. Langacker, arXiv:0911.4294.
[28] S. Gopalakrishna, T. Han, I. Lewis, Z.-g. Si, and Y.-F. Zhou, Phys. Rev. D **82**, 115020 (2010).
[29] J. H. Kühn and G. Rodrigo, Phys. Rev. Lett. **81**, 49 (1998).
[30] J. H. Kühn and G. Rodrigo, Phys. Rev. D **59**, 054017 (1999).
[31] O. Antuñano, J. H. Kühn, and G. Rodrigo, Phys. Rev. D **77**, 014003 (2008).
[32] P. Ferrario and G. Rodrigo, Phys. Rev. D **78**, 094018 (2008).
[33] Y.-k. Wang, B. Xiao, and S.-h. Zhu, Phys. Rev. D **82**, 094011 (2010).
[34] Y.-k. Wang, B. Xiao, and S.-h. Zhu, Phys. Rev. D **83**, 015002 (2011).
[35] B. Xiao, Y.-K. Wang, Z.-Q. Zhou, and S.-h. Zhu, Phys. Rev. D **83**, 057503 (2011).
[36] T. Aaltonen *et al.* (CDF Collaboration), arXiv:1101.0034.